

# Magnetocaloric effect for a $Q$ -clock type system

Michel Aguilera,<sup>1,2,\*</sup> Sergio Pino-Alarcón,<sup>2</sup> Francisco J. Peña,<sup>2,3,†</sup> Eugenio E. Vogel,<sup>4,5,6</sup> and Patricio Vargas<sup>7</sup>

<sup>1</sup>*Instituto de Física, Pontificia Universidad Católica de Valparaíso, Casilla 4950, Valparaíso 2373223, Chile*

<sup>2</sup>*Departamento de Física, Universidad Técnica Federico Santa María, Valparaíso 2390123, Chile*

<sup>3</sup>*Millennium Nucleus in NanoBioPhysics (NNBP), Av. España 1680, Valparaíso 2390123, Chile*

<sup>4</sup>*Departamento de Ciencias Físicas, Universidad de La Frontera, Casilla 54-D, Temuco, Chile*

<sup>5</sup>*Center for the Development of Nanoscience and Nanotechnology, Santiago 9170124, Chile*

<sup>6</sup>*School of Engineering, Central University of Chile, Santiago, Chile*

<sup>7</sup>*Departamento de Física, CEDENNA, Universidad Técnica Federico Santa María, Av. España 1680, Valparaíso 2390123, Chile*

(Dated: May 24, 2024)

In this work, we study the magnetocaloric effect applied to a magnetic working substance corresponding to a square lattice of spins with  $Q$  possible orientations known as the “ $Q$ -state clock model” where for  $Q \geq 5$ , the systems present the famous Berezinskii–Kosterlitz–Thouless phase (BKT). Thermodynamic quantities are obtained in exact form for a small lattice size of  $L \times L$  with  $L = 3$  and by the mean-field approximation and Monte Carlo simulations for  $Q$  pairs between 2 and 8 with  $L = 3, 8, 16, 32$  with free boundary conditions, and magnetic fields varying between  $B = 0$  and 1 in natural units of the system. By obtaining the entropy, it is possible to quantify the caloric effect through an isothermal process in which the external magnetic field on the spin system is varied. In particular, we find the values of  $Q$  that maximize the effect depending on the lattice size and the magnetic phase transitions related to maximizing the caloric phenomena. These indicate that in a small lattice (up to  $\sim 7 \times 7$ ), when  $Q \geq 5$ , the transition that maximizes the effect is related to ferromagnetic to BKT type. In contrast, transitioning from BKT to paramagnetic type increases the system’s caloric response when we work with a larger lattice size.

## I. INTRODUCTION

The caloric phenomena constitute a fundamental axis of study in the physics of materials to find replacement candidates for the toxic gases used in conventional refrigeration systems [1, 2]. To this end, considerable temperature variations have been achieved for different types of materials after an adiabatic variation of the value of the applied hydrostatic pressure (barocaloric effect) [3–6], mechanical stress (elastocaloric effect) [7–11], electric field (electrocaloric effect) [12–15] and external magnetic field (magneto-caloric effect, MCE) [16–19]. Although each phenomenon’s nature and physical interpretation are different, they comply with a basic concept that characterizes them: the aim is to maximize the variation of entropy in the face of changes in the control parameter that governs the thermodynamic process that describes the phenomenon [20–26]. In particular, the systems that present phase transitions maximize entropy variation near the transition [27–30]. One of many corresponds to magnetic materials, characterized by a determined magnetic order or ground state. Remarkably, such an order depends on the energy contributions in the material [31–33]. Within these transitions, we will focus on those magnetic systems that present as the temperature increases and thus change their magnetic phase. An interesting system to explore corresponds to the  $Q$ -state clock model that constitutes the discrete version of the famous 2D XY model [34–37], which is probably the

most extensively studied example showing the Berezinskii–Kosterlitz–Thouless (BKT) transition in the presence of a frustrated quenched disordered phase [38–40]. The  $Q$ -state clock model is one of many magnetic models to mimic the thermodynamics of some materials, and it can be viewed as a classical Heisenberg spins model with very strong planar anisotropy [41–43].

One way to characterize the phase transitions of the  $Q$ -clock state model is through the maxima obtained in the specific heat as a function of temperature. Each location of a maximum of the specific heat on the temperature axis will represent a value for a so-called *critical temperature*. It has been shown [44–49] (in the absence of an external magnetic field) that for the  $Q$ -clock state model, values  $Q \geq 5$  (where  $Q$  represents the number of possible orientations that the spins can take), the specific heat presents two maxima. The first maximum corresponds to transitioning from a ferromagnetic phase (FP) to a BKT phase. In contrast, the second maximum transitions from BKT to a paramagnetic disordered phase (PP) [36].

In this sense, this model, which presents these two phase transitions mentioned above, is very interesting to exploit in studying caloric phenomena. In addition, applying this spin model to this effect raises several questions: which value of  $Q$  is the optimum, i.e., maximizes the thermodynamic response? How does the estimation of the magnitude of the effect through mean-field approximation compare to the exact calculations and Monte Carlo simulations? Is it possible to know which magnetic phases maximize the effect? Is there convergence in the results when we increase the size of the lattice?

One of the technical difficulties with this model is the scaling of the accessible states, which scales as  $\sim Q^{L^2}$

\* [michel.aguilera@usm.cl](mailto:michel.aguilera@usm.cl)

† [francisco.penar@usm.cl](mailto:francisco.penar@usm.cl)

where  $L \times L$  represents the size of the lattice you work. This means that when solving thermodynamics exactly via a canonical partition function, the computational costs result in long computation times. With this limitation, exact model computations can only be applied to lattices of small size. That is why two relevant mechanisms are employed to see what happens with larger lattices: Mean field approximation and Monte Carlo simulations.

In this work, we study the MCE in the  $Q$ -clock model, in which the thermodynamic quantities of the model are obtained exactly for small lattices and using a mean-field approximation and Monte Carlo simulations for larger lattice sizes. The  $Q$  values studied correspond to the even values  $Q = 2, 4, 6$  and  $8$ . The exact calculation for a small lattice of  $L \times L$  with  $L = 3$  is presented to review the MCE concerning the magnetic phase and to quantify the caloric effect per spin of small-size lattices. In completeness, the results are analyzed using the mean-field approximation of this lattice to verify if the estimates in the orders of magnitude of the effect are consistent with this approximation. Finally, our analysis is extended to  $16 \times 16$  and  $32 \times 32$  lattices employing a mean-field and Monte Carlo simulations.

Our work is structured as follows: Section II presents the  $Q$ -clock model, Section III revisits the mean-field approximation, Section IV analyzes the thermodynamic quantities involved in the calculations, Section V gives an analysis of the caloric phenomena, Section VI shows the results, and finally, Section VII presents our work's conclusions.

## II. SPIN MODEL

### A. $Q$ -state clock model

The working substance under study corresponds to the  $Q$ -states clock model on a two-dimensional (2D) square lattice of dimensions  $L \times L = N$ , where the local magnetic moment or "spin"  $S_i$  at site  $i$  can point in any of  $Q$  directions in a given plane.  $S_i$  is then a 2D vector, i.e.  $S_i = (\cos(\frac{2\pi}{Q}k), \sin(\frac{2\pi}{Q}k))$ , where  $k = 0, 1, \dots, Q-1$ , with equal probability. The magnitude of  $S_i$  is chosen as the unity.

The isotropic Hamiltonian for such a system can be written as:

$$\mathcal{H} = - \sum_{\langle i,j \rangle} \mathcal{J}(\vec{S}_i \cdot \vec{S}_j) - \sum_i \vec{B} \cdot \vec{S}_i, \quad (1)$$

where  $\mathcal{J} > 0$  is the ferromagnetic exchange interaction to nearest neighbors; the sum runs over all pairs of nearest neighbors  $(i, j)$ , which is indicated by the symbol  $\langle i, j \rangle$  under the summation symbol.  $\vec{B}$  is an external field applied along one direction in the plane. In this work, we used arbitrary units choosing  $\mathcal{J} = 1$ , making all the calculated quantities for the exchange energy constant.

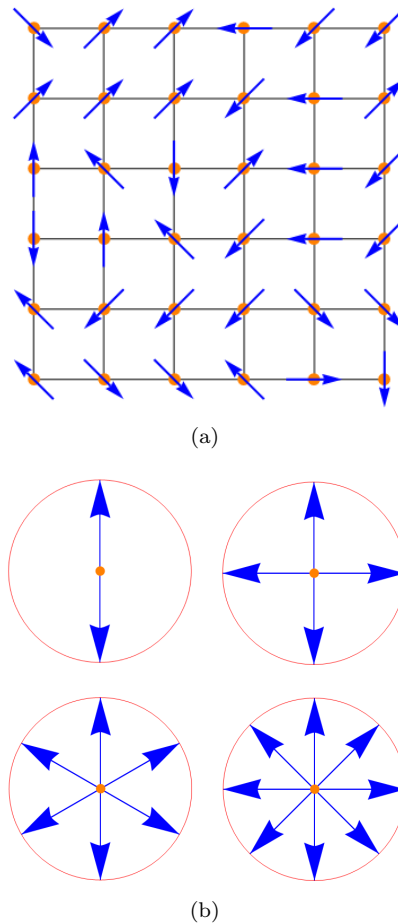


FIG. 1. (a)  $6 \times 6$  spin lattice and (b)  $Q$  clock model for  $Q = 2, 4, 6$  and  $8$ .

From this Hamiltonian model, we must extract the accessible states of the system to obtain the entropy of the system.

To quantify the caloric effect, it is necessary to obtain the entropy from the thermodynamic study of the model. We will first analyze two cases where this calculation comes from a canonical partition function. The first corresponds to an exact calculation of all the accessible microstates of the system for a  $3 \times 3$  lattice for  $Q = 2, 4, 6$  and  $8$ . For the same values of  $Q$  studied, the mean-field theory will be employed for lattices of size up to  $32 \times 32$ . On the other hand, Monte Carlo simulations offer us the possibility to obtain thermal averages with a sample of the configurations and to define an entropy via integration of the specific heat.

In the next section, we will review the mean-field approximation to emphasize the calculation of the approximate partition function and the definition taken from there for the entropy coming from the Helmholtz free energy temperature derivative, which also applies to the exact case in small lattices.

### III. MEAN FIELD APPROXIMATION

The mean-field theory assumes that the fluctuations around the average value of the order parameter, in this case, the magnetization per site  $\vec{m} = \vec{M}/N$ , are so small that they can be neglected. The first term of the Hamiltonian of Eq. (1) that corresponds to the interaction term between the spin of the lattice in different sites is modified by performing the following approximations.

We can write the spin term as follows:

$$\vec{S}_j = \vec{m} + \delta\vec{S}_j, \quad (2)$$

where  $\vec{m}$  is the average thermodynamic spin, the same for all sites in the lattice. Therefore, we have

$$\delta\vec{S}_j = \vec{S}_j - \vec{m}_j. \quad (3)$$

Thus, the spin-spin interaction term can be written as

$$\vec{S}_i \cdot \vec{S}_j = -m^2 + \vec{m} \cdot (\vec{S}_i + \vec{S}_j), \quad (4)$$

where we have neglected the square terms of the fluctuation ( $O(\delta\vec{S})^2$ ). Therefore, the interaction term of the Hamiltonian of Eq. (1) (that we call  $\mathcal{H}_J$ ) can take the form

$$\begin{aligned} \mathcal{H}_J &= -\mathcal{J} \sum_{\langle i,j \rangle} \left( -m^2 + \vec{m} \cdot (\vec{S}_i + \vec{S}_j) \right) \\ &= \sum_i (2\mathcal{J}m^2 - \mathcal{J}z\vec{m} \cdot \vec{S}_i), \end{aligned} \quad (5)$$

where now the sum runs for each site in the lattice, and  $z$  are the effective nearest neighbors of the model. Consequently, we can define a Hamiltonian per site given by the structure

$$h_i = \frac{z}{2}\mathcal{J}m^2 - \mathcal{J}z\vec{m}_i \cdot \vec{S}_i - \vec{B} \cdot \vec{S}_i. \quad (6)$$

Now, we can calculate the partition function per site, which will depend on  $Q$ ,  $B$ ,  $m$  and  $T$  given by

$$Z(q, B, m, T) = \sum_q e^{-\frac{\xi(q, B, m)}{T}}, \quad (7)$$

where  $\xi(q, B, m)$  is the energy per site coming from the Hamiltonian of Eq. (6).

To extrapolate the results of mean field approximation of the thermodynamic quantities in smaller lattices, in the Ref. [43], we discuss the idea of finding an effective nearest neighbor ( $z_{eff}$ ) through a simple optimization protocol. This protocol matches the internal energies obtained for a lattice of  $L \times L$  with  $L = 3$  employing exact

and mean-field calculations. In this way, by releasing the number of neighbors,  $z_{eff} \in \mathbb{R}^+$ , and minimizing the internal energy difference (between the exact and approximate case via mean-field), it was found that for  $L = 3$ , the optimal number of neighbors was  $z_{eff} = 2.67$  (for all values of  $Q$ ).

Amplifying the above qualitatively, we propose an expression for the number of near neighbors effective that adjusts according to the weighting of the effect of non-interacting edges in the system when the lattice has a generic resolution  $L \times L$ . The effective neighbors for a central spin for the mean-field are determined by the following expression (independent of  $Q$ ) for the square lattice with up, down, left, and right near neighbors [43]

$$z_{eff} = \frac{4 \times (L - 2)^2 + 3 \times 4 \times (L - 2) + 2 \times 4}{L^2}. \quad (8)$$

### IV. THERMODYNAMIC QUANTITIES

Once the partition function of the system has been obtained by either of the two approaches discussed above, it is possible to compute all the thermodynamical observables in a general way through the expressions ( with  $k_B = 1$  )

$$F = -T \ln Z, \quad (9)$$

$$U = T^2 \frac{\partial \ln Z}{\partial T}, \quad (10)$$

and

$$C = \frac{\partial U}{\partial T}, \quad (11)$$

where  $F$  is the Helmholtz free energy,  $U$  is the internal energy and  $C$  is the specific heat at constant magnetic field. In addition, with the differential expression of Helmholtz free energy given by  $dF = -SdT - MdB$ , we can obtain the entropy and the magnetization of the system given by

$$S = -\frac{\partial F}{\partial T}; \quad M = -\frac{\partial F}{\partial B}. \quad (12)$$

We will begin by reviewing the thermodynamic results of the model, focusing first on the analysis of the specific heat for the exact results of a  $3 \times 3$  lattice. This thermodynamic quantity for a field  $B = 0.05$  and field  $B = 1$  is shown in Fig. 2(a) and Fig. 2(b), respectively for  $Q = 2, 4, 6, 8$ . Here, we observe two peaks for  $q \geq 6$ , indicative of a double-phase transition. It is, therefore, the BKT phase that appears in these cases. It is also noticeable that the critical temperature of each transition

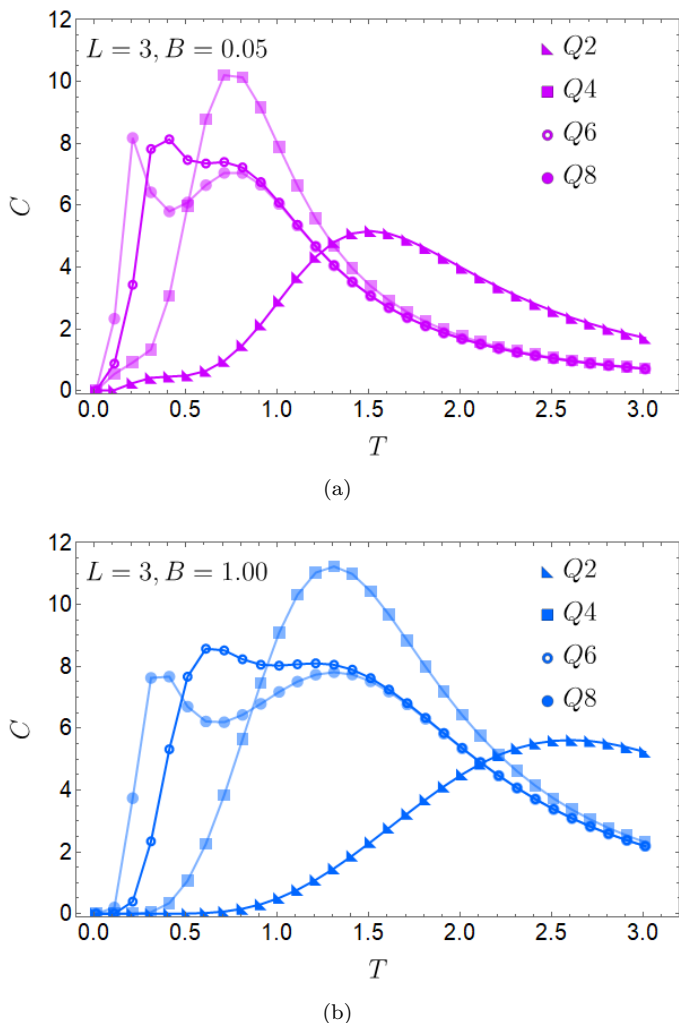


FIG. 2. Specific heat as a function of temperature for even  $Q$  values between  $Q = 2$  and  $Q = 8$  for (a)  $B = 0.05$  and (b)  $B = 0.1$  for a  $3 \times 3$  lattice. We observe the peak displacements to the right at a higher magnetic field.

increases with the increasing external field, as we can observe from Fig. 2(b) compared with the critical temperatures obtained for (a) panel of the same figure. This is because the external field favors ordered phases (FM and BKT) over disordered ones. A different behavior is obtained by fixing the field and increasing  $Q$ , where we observe that the high-temperature peak remains at the same temperature, whereas the low-temperature peak tends toward lower temperatures (eventually to a zero temperature) as  $Q$  increases, tending to infinity. Therefore, for  $Q \rightarrow \infty$ , we expect the temperature of the first transition (from FM to BKT phase) to go to zero. The case of internal energy is shown in Fig. 3(a), where we observe that we obtain lower values for the case with a magnetic field than for the case without an external magnetic field. This is due to the Zeeman term present in the Hamiltonian given by Eq. (1), which decreases the ground state energy compared to the case in the absence

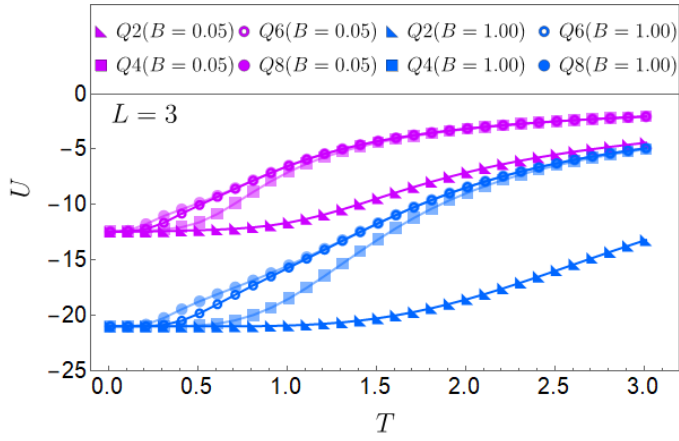
of a magnetic field. Continuing with the thermodynamic description of our system of study, Fig. 3(b) shows the magnetization of the system for  $Q = 2, 4, 6$ , and  $8$  for high fields  $B = 1$  (blue curves) and  $B = 0.05$  (purple curves). First, we notice that all systems start saturated (in a ferromagnetic state) and then decrease their magnetization as the temperature increases. The case with a higher external magnetic field shows higher magnetization than the case with a lower magnetic field as the temperature increases for all  $Q$  displayed. It is observed that the change in magnetization as a function of temperature happens much faster for larger and larger  $q$  values. This is a direct consequence of the degrees of freedom of the system. For example, we can think of  $Q = 2$ , where two possible orientations are up and down. In terms of energy, generating a flip of such a configuration is much more difficult. Therefore, the magnetization at the same temperature will be higher than in the other cases for higher values of  $Q$ .

Next, we analyze the entropy in Fig. 3(c). We observe that for a given  $Q$ , the entropy is lower for the case with field  $B = 1$  than for the case of  $B = 0.05$ . This is consistent with the interpretation that the magnetic field tends to order the spin system. Also, it is noticeable that for more spin degrees of freedom (as  $Q$  increases), the entropy is higher as a function of temperature consistent with the greater number of accessible states the system acquires. These graphs show that the entropy fulfills that  $\lim_{T \rightarrow 0} S(T, B \neq 0) = 0$  because, with even a very low field value, the system at low temperature tends to have only one preferred state due to the presence of the external field applied to the system. It is important to remember that in the case of a null field, the entropy at low temperature has the value of  $\lim_{T \rightarrow 0} S(T, 0) = \ln Q$ .

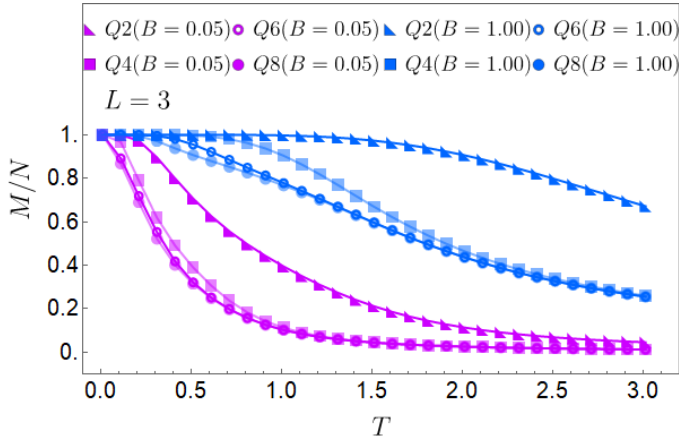
In Fig. 4(a), we note the saturation in the magnetization for low temperatures, finding for all the cases studied the unity for the limit of  $T \rightarrow 0$ . Additionally, we observe that the temperature increase increases the difference between the mean field and the exact calculation for the Ising case ( $Q = 2$ ). In contrast, for  $Q \geq 4$ , the difference between both methods decreases as the temperature increases. In Fig. 4(b), we find the spin magnetization of a  $3 \times 3$  lattice with an external magnetic field close to zero ( $B = 0.05$  in  $\mathcal{J}$  units) for different values of  $Q = 2, 4, 6, 8$  calculated in an exact way (purple color) and approximated via mean field (green color). We note a difference in the shape of the curves as the temperature increases, although both methods start to become saturated at low temperatures. The shape of the exact calculated curve shows that the magnetization behavior for low non-zero external fields varies with increasing field and not so for the medium field case.

## V. CALORIC PHENOMENA

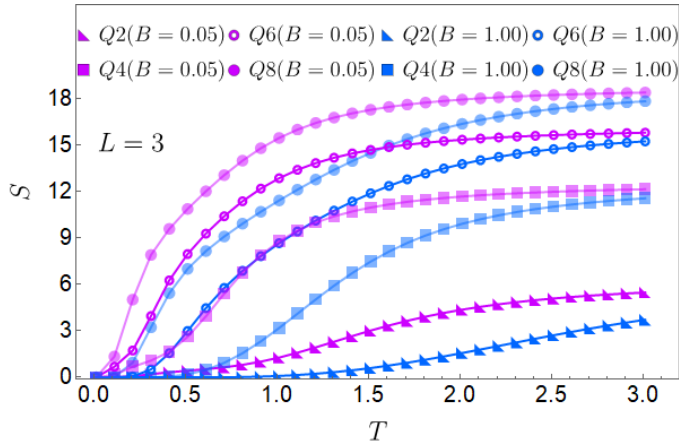
To analyze this effect, we start by treating the total entropy of a material as the sum of three entropies: elec-



(a)

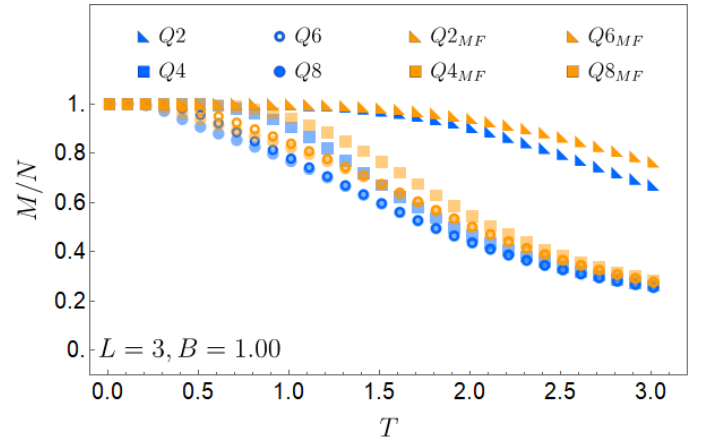


(b)

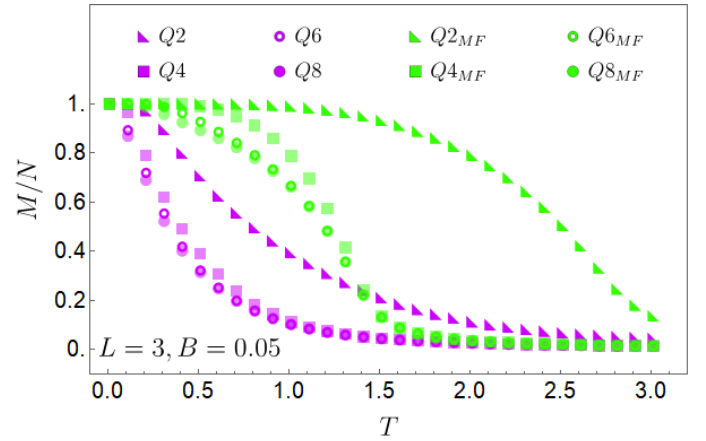


(c)

FIG. 3. Internal energy (a), magnetization (b), and entropy (c) as a function of temperature for different values of  $Q$  pairs between  $Q = 2$  and  $Q = 8$  for fields  $B = 0.05$  (purple) and  $B = 0.1$  (blue) for a  $3 \times 3$  lattice.



(a)



(b)

FIG. 4. In panel (a), we show the spin magnetization of a  $3 \times 3$  lattice with an external magnetic field equal to unity for different values of  $Q = 2, 4, 6, 8$  calculated exactly (orange color) and approximated via mean field (blue color). In panel (b), we exhibit the spin magnetization of a  $3 \times 3$  lattice with an external magnetic field close to zero ( $B = 0.05$  in  $\mathcal{J}$  units) for different values of  $Q = 2, 4, 6, 8$  calculated exactly (purple color) and approximated via mean field (green color).

tronic  $S_e$ , magnetic  $S_m$ , and lattice  $S_l$ .

$$S(T, B) = S_e(T, B) + S_m(T, B) + S_l(T, B) \quad (13)$$

Magnetic entropy depends strongly on the magnetic field, whereas it is very common to find materials with electronic and lattice entropy with negligible dependence on the magnetic field. However, this is not general, and we highlight that in a low temperatures regime ( $\approx < 10$  K), some reports indicate that the electronic entropy can present nonlinear dependence on the magnetic field. In this work, let us assume that we are dealing with a more usual system, where we can establish null dependence of the magnetic field in the lattice and electronic entropies so that Eq. (13) is of the form:

$$S(T, B) \approx S_e(T) + S_m(T, B) + S_l(T) \quad (14)$$

The quantification of the caloric phenomenon is associated with a thermodynamic refrigerator cycle, where we can take two paths to quantify the effect: i) an adiabatic trajectory and ii) an isothermal trajectory. The temperature variation that suffers the systems along the isentropic process is called  $\Delta T_{ad}$  and is given by the expression

$$\Delta T_{ad} = - \int_{B_i}^{B_f} \frac{T}{C_B} \left( \frac{\partial S}{\partial B} \right)_T dB, \quad (15)$$

where we use that  $C_B = \left( \frac{\partial U}{\partial T} \right)_B = T \left( \frac{\partial S}{\partial T} \right)_B$  corresponds to specific heat at constant  $B$  parameter.

In the case of quantifying the effect employing an isothermal trajectory, we obtain an entropy variation at constant temperature ( $\Delta S$ ) given by

$$\Delta S = \int_{B_1}^{B_2} \left( \frac{\partial S}{\partial B} \right)_T dB. \quad (16)$$

The quantity  $\left( \frac{\partial S}{\partial B} \right)_T$  that appears in the last two equations can be rewritten in terms of the magnetization of the system via Maxwell's relationship  $\left( \frac{\partial S}{\partial B} \right)_T = \left( \frac{\partial M}{\partial T} \right)_B$ .

If we look at Eq. (15) and Eq. (16), we can find a relationship between these quantities concerning each other. It is found that  $-\Delta S \propto \Delta T_{ad}$ . Consequently, it is essential to note that when you have a case in which  $-\Delta S > 0$ , let's call this kind of response of direct type. The system will heat up, while when the response is of the  $-\Delta S < 0$  type, we call this inverse type response, and consequently, the system will cool down. Therefore, we expect for direct response a  $\Delta T_{ad} > 0$ , and for the case of an inverse response, we expect a  $\Delta T_{ad} < 0$  for the final result of the caloric phenomena.

For the case of the entropy variation at constant temperature ( $T$ ), the expression can be given by the difference of the entropy at the initial and final point of the process in the following form:

$$-\Delta S = -\Delta S_m = S_m(T, B_0) - S_m(T, B), \quad (17)$$

where the contributions of  $S_l$  and  $S_e$  have been canceled due to its dependence only on temperature, and consequently, in an isothermal process, it will have no associated variations. The last equation generates a graph for a given  $B_0$  and final  $B$  as a function of  $T_0$  that quantifies the caloric phenomena.

## VI. RESULTS

To start the discussion of the caloric phenomena, we must fix the zero value for temperature and the external

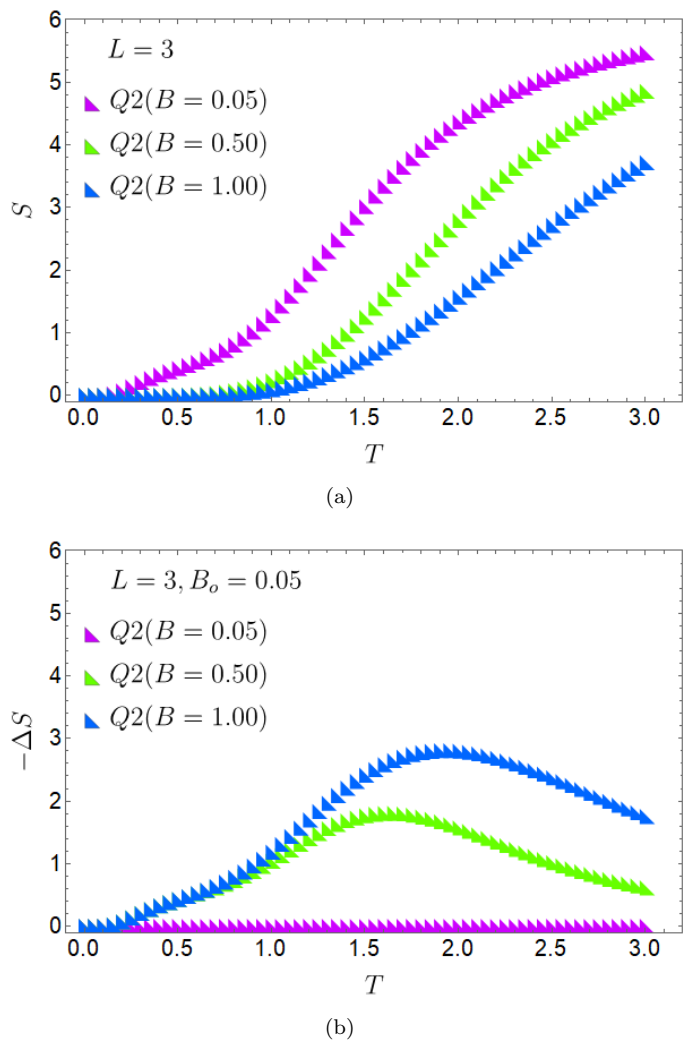


FIG. 5. (a) Entropy as a function of temperature for the case  $Q = 2$  for the case of  $B = 0.05$  (purple curve),  $B = 0.5$  (green curve) and  $B = 1$  (blue curve). (b) Entropy difference  $-\Delta S = S(T, B_0 = 0.05) - S(T, B)$  as a function of temperature for  $B = 0.5$  (green curve),  $B = 1$  (blue curve) and  $B = 0.05$  (purple curve).

magnetic field for our calculations. The zero temperature for our thermodynamic quantities will be  $T = 0.01$  while the smallest field we will work with will be  $B = 0.05$ . These two quantities combined produce zero entropy, as theoretically expected. In addition, the selection of  $B = 0.05$  as the lowest field is supported to avoid the problem generated when we have  $B \rightarrow 0$  in the mean-field self-consistency equation. Regarding the maxima used in our calculations, the maximum temperature corresponds to  $T = 3.01$  and  $B = 1$  in units of  $\mathcal{J}$ , both quantities.

### A. Small Lattices

Let us start the analysis with a simple example of the exact case ( $3 \times 3$  lattice) for  $Q = 2$  to understand the

caloric response of the system. For this purpose, we plotted the entropy for three different field values of the system in Fig. 5(a), where  $B = 0.05$  is the purple curve,  $B = 0.5$  is the green curve, and  $B=1$  is the blue curve. The entropy difference that quantifies the effect is given by  $-\Delta S = S(T, 0.05) - S(T, B)$ , where we have selected the initial point with an external field strength  $B = 0.05$ . These entropy differences can be plotted for different field values on a curve as a function of the temperature to which the process is taken, and they are presented in Fig. 5(b). From this last figure, we note that the response of the effect is positive, which indicates a direct type of behavior for both cases presented. It is also observed that below 0.9 temperature (approximately), the thermal response of the effect for  $B = 0.5$  and  $B = 1$  are equal. After this temperature value, it is observed that the case with the higher field is notably different from the one with a lower field. The explanation of this phenomenon is relatively simple. The system prefers to be in a ferromagnetic configuration in an external magnetic field, i.e., in a single configuration state. To remove it from this state requires a considerable increase in temperature in terms of energy. This is reflected in the entropy for cases  $B = 0.5$  (green curve) and  $B = 1$  (blue curve) in Fig. 5(a) where both entropies are equal up to  $T \sim 0.9$  and then differentiate with  $B = 0.5$  being higher than  $B = 1.0$ .

To compare the effects for the exact calculations and mean field, we have analyzed  $-\Delta S$  for the case of a final field of  $B = 0.1$  and  $B = 1$  and the initial fixed value of field  $B = 0.05$ . From Fig. 6(a), we note a large discrepancy in the effect's location as a temperature function for the case with a final  $B$  of 0.1. As we observe in Fig. 6(b), this discrepancy decreases as we increase the final field. It is remarkable from these two comparative plots that if we only focus on estimating the maximum effect at the value associated only with  $-\Delta S$  and not the location of the temperature, both calculations do not differ too much. We will return to this point later in the discussion when we deal with other  $Q$  cases.

We will now analyze the MCE for different values of  $Q$  of the  $3 \times 3$  lattice, both in the exact case and using the mean field. This is presented in Fig. 7, where the cases for a final field of  $B = 0.1$  (panel (a)) and the case of  $B = 1$  (panel (b)) with an initial field of  $B = 0.05$  are shown. We first notice that for the value of  $Q = 4$ , what was observed for  $Q = 2$ , associated with the location of the maximum temperature effect for both methods, is also true. As the magnetic field increases, the maximum temperature locations become closer. However, a considerable error is obtained when extrapolating mean-field solutions for small lattices, and it has to do with the location of the maximum (or maxima) at  $-\Delta S$  when we have the cases  $Q = 6$  and  $Q = 8$  as we can appreciate in Fig. 7(b). From this last figure, it can be seen that both  $Q = 6$  and  $Q = 8$  present two maxima in  $-\Delta S$ , vestiges of the double transition present for those values of  $Q$  in the model, both for the mean field and the exact calculations. We note that

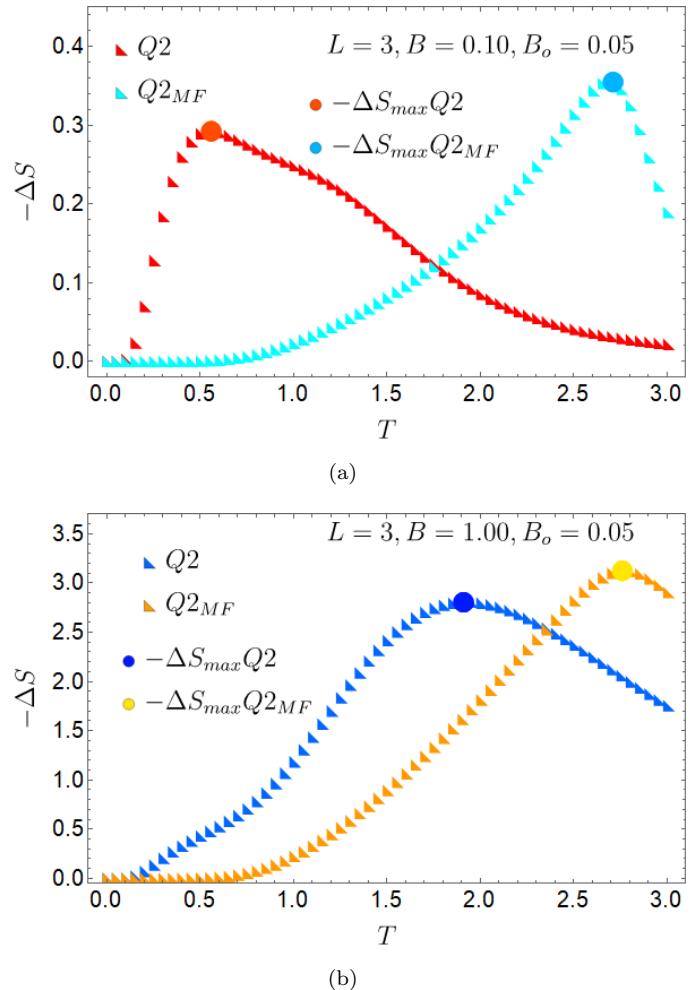
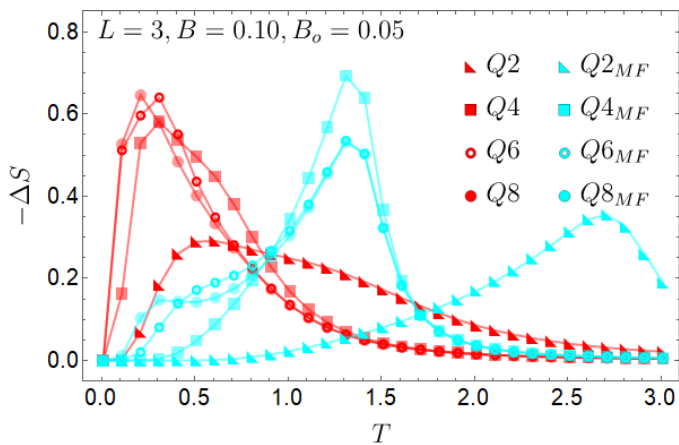
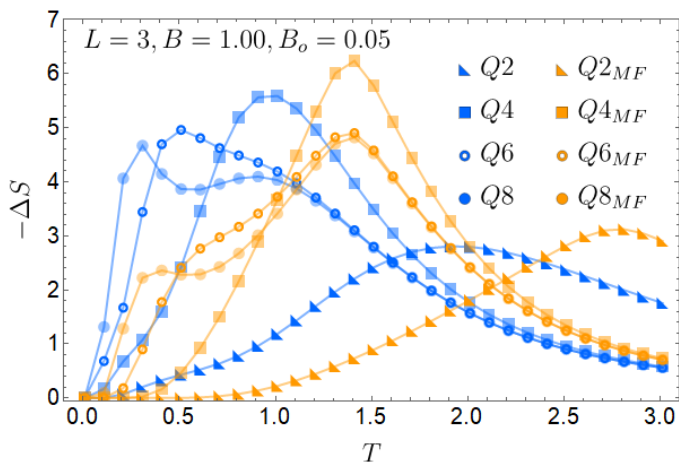


FIG. 6. Caloric response with an initial  $B$  of 0.05 for the case of a final field of (a)  $B = 0.1$  and (b)  $B = 1$  for exact calculations for a  $3 \times 3$  lattice and using the mean-field approximation.

the exact calculations indicate that the peak at the lowest temperature is where the greatest effect occurs, while the mean field indicates the opposite; the second peak indicates the maximum value of the effect. Our previous work [41, 42] shows this phenomenon in the specific heat up to lattice of approximately  $7 \times 7$ . After that value, the second peak observed in the specific heat becomes larger, following the trend shown and observed in the mean-field approximation. In addition, from Fig. 7(a), we observe that in the exact case for the same parameter and lattice configuration, the maximum of the effect is slightly higher for  $Q = 6$  and  $8$  than for  $Q = 4$ . Meanwhile, the mean-field indicates that the ordering of the effect from highest to lowest is  $Q = 4$ ,  $Q = 6$ ,  $Q = 8$ , and finally,  $Q = 2$ . In contrast, from Fig. 7(b), we can see that the largest effect is obtained for  $Q = 4$  independent of the calculation method. This is remarkable since previous studies found that when applying thermodynamic cycles using the  $Q$ -clock model as the working substance, the



(a)



(b)

FIG. 7. Caloric response for a  $3 \times 3$  lattice with an initial field of  $B=0.05$  and a final field of (a)  $B = 0.1$  and (b)  $B = 1$  for the exact and mean field cases for  $Q = 2, 4, 6$  and  $8$ .

maximum efficiency and useful work are obtained for the parameter  $Q = 4$  [43]. These two cases, therefore, indicate that there is a field value at which this inversion observed in the effect maxima occurs. For this purpose, we plot in Fig. 8 the value of the maximum  $-\Delta S_{max}$  as a function of the field independent of the location in temperature at which it occurs both for the mean field and for the exact calculation. From this plot, we can notice that in the exact case,  $Q = 6$  and  $Q = 8$ , responses higher than  $Q = 4$  and  $Q = 2$  are observed up to a field of approximately  $\sim 0.26$ . After that value, the effect is ordered in the same way as the mean-field results, i.e., in the form:

$$-\Delta S_{max}^{Q=4} > -\Delta S_{max}^{Q=6} > -\Delta S_{max}^{Q=8} > -\Delta S_{max}^{Q=2}, \quad (18)$$

equation valid only for a final  $B > 0.26$ .

From Fig. 8, we can also confirm what happens when estimating the maximum effect between the exact and

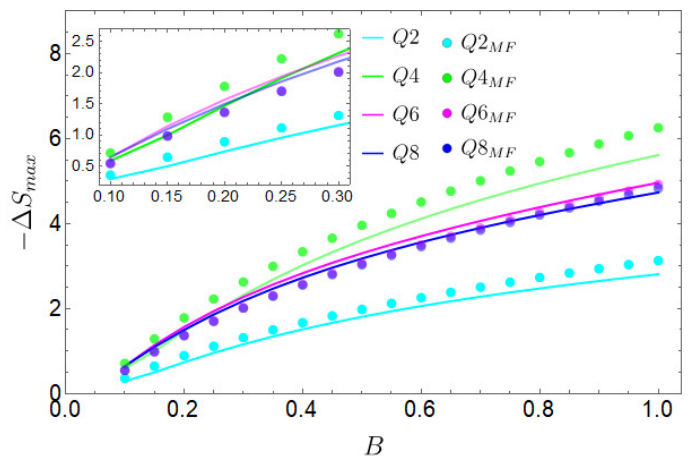


FIG. 8. Maximum caloric response ( $-\Delta S_{max}$ ) as a function of the applied external field between 0.1 and 1.0 for a  $3 \times 3$  lattice with an initial magnetic field  $B = 0.05$  for  $Q = 2, 4, 6$  and  $8$  employing exact calculations (solid lines) and mean field calculations (dashed lines).

mean-field calculations. Although the mean-field and exact differ quite a bit in the temperature location of the maximum point, if we focus only on the numerical value of effect maximization at  $-\Delta S$ , the mean-field does not show significant variations compared to the exact calculation even for a small lattice, as shown in this study. The dotted curves in Fig. 8 representing mean-field calculations differ very little from the solid lines of the exact case, with the largest difference observed for  $Q = 4$  and the smallest differences for  $Q = 6$  and  $Q = 8$ . From this tendency, we can conclude that for values larger than  $Q = 4$ , the numerical estimate of  $-\Delta S$  will be closer between the two methods presented. We can say, then, that the mean field is useful in this context even for small lattices in the numerical estimation of the maximum effect but fails logically in the location of the temperature where it occurs because the nature of the approximation used is regularly employed for lattices of larger sizes.

An interesting point to discuss is the location in temperature where the maximum value of the effect is given compared to the critical temperature ( $T_c$ ) of the different phases present in the model. This is shown in Fig. 9, which represents a plot of  $T$  vs.  $B$  for (a)  $Q = 2$  and  $Q = 4$  and for (b)  $Q = 6$  and  $Q = 8$ . To understand these plots, we will start with the cases  $Q = 2$  and  $Q = 4$  presented in Fig. 9(a). We must think that the variation of the effect is given by  $-\Delta S = S(T, B_0 = 0.05) - S(T, B)$  and hence is described by a spin system starting with an entropy of the form  $S(T, B_0 = 0.05)$ . This quantity has associated a specific heat  $C(T, B_0 = 0.05)$  that defines a critical temperature represented by horizontal lines in Fig 9(a). On the other hand, the continuous lines represent the final entropy state  $S(T, B)$ , which has an associated specific heat  $C(T, B)$ , which will deliver as the field changes different critical temperature values, indicating the respective phase transition for these cases.

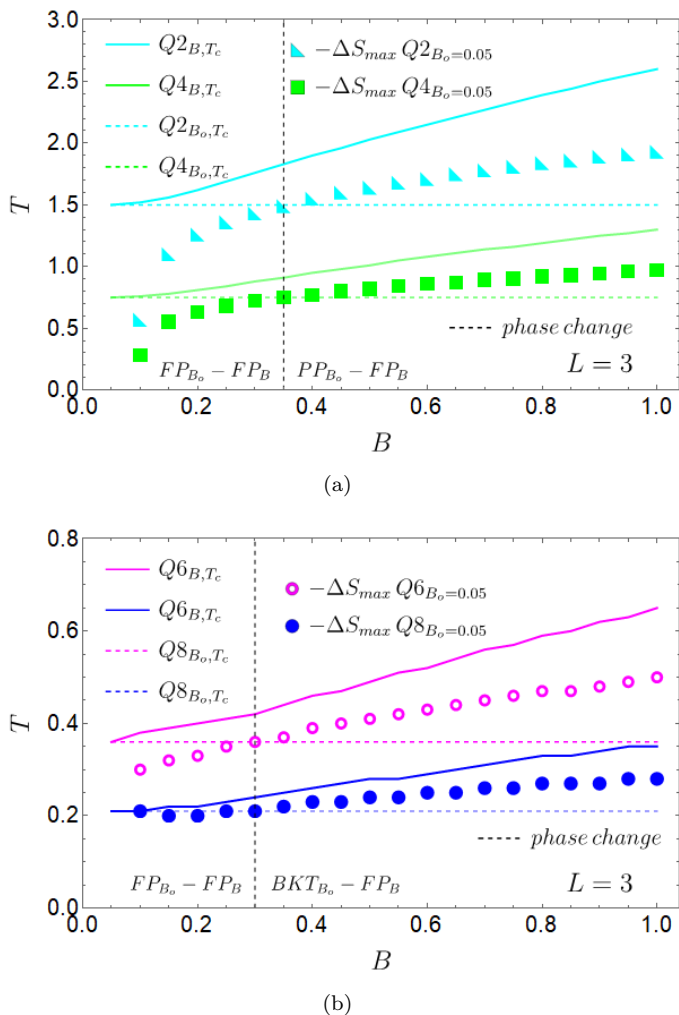


FIG. 9.  $T$  vs.  $B$  phase diagram for (a)  $Q = 2$  and  $Q = 4$  and for (b)  $Q = 6$  and  $Q = 8$ . The solid lines for (a) represent the critical temperatures of the FP-PP type transition of the final state of the spin system  $S(T, B)$ , while for (b), the solid lines represent the critical temperatures of the FP-BKT type transition of the final state of the spin system  $S(T, B)$ . For (a), the light blue triangles indicate the maximum obtained from  $-\Delta S = S(T, B_0 = 0.05) - S(T, B)$  with  $Q = 2$  and the green squares indicate the same but for  $Q = 4$ . The same applies to  $Q = 6$  represented by magenta circles and  $Q = 8$  with blue circles. The horizontal dotted lines indicate the critical temperature of the  $S(T, B_0 = 0.05)$  state for  $Q = 2$  (light blue),  $Q = 4$  (green),  $Q = 6$  (magenta) and  $Q = 8$  (blue). The black vertical dotted lines (for panels (a) and (b)) represent the location where the systems maximize  $-\Delta S$  passing through an effective phase change.

The graphs with geometrical figures (triangular for  $Q = 2$  and square for  $Q = 4$ ) are the points where, for a given field,  $-\Delta S$  is the maximum. Precisely, the intersection between the curve with geometric figures and the dotted horizontal one generates, for  $Q = 2$  and  $Q = 4$ , two possible regions where the system maximizes its effect. Under a field value given by the vertical black line, the

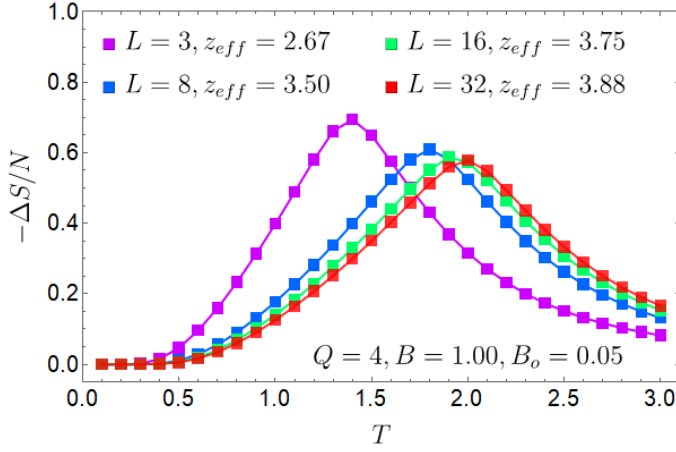
system maximizes its effect in a region where the system starts in a ferromagnetic phase ( $FP_{B_0}$ ) and ends in a ferromagnetic phase ( $FP_B$ ) while past that critical field value found the system maximizes the caloric response starting from a paramagnetic phase ( $PP_{B_0}$ ) and ending in a ferromagnetic phase ( $FP_B$ ).

The same analysis can be made if we recall that for the exact case of  $Q = 6$  and  $Q = 8$ , the peak of the effect was concentrated in the first peak of Fig. 7 and, therefore, more oriented to transitions relating to the BKT and FP phases. This is shown in Fig. 9(b), where the maxima are concentrated when the system remains in a ferromagnetic phase or involves transitions linking the BKT and FP phases. We note that the maxima of the effect for  $Q = 8$  are much closer to the  $T_c$  of the first phase transition related to an FP-BKT type transition of the final state of the spin system than what occurs for the case of  $Q = 6$ .

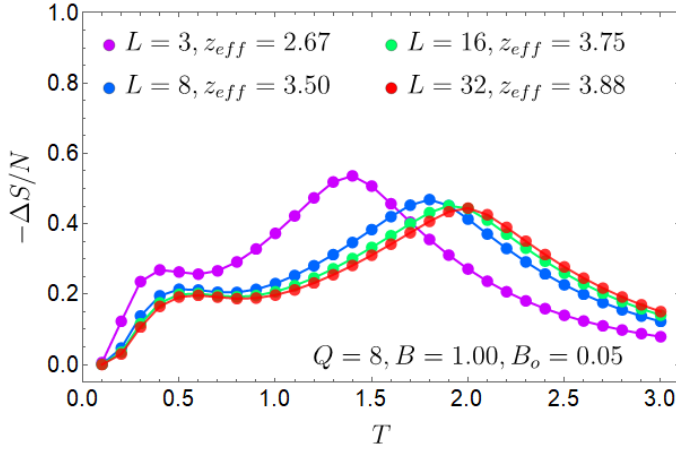
## B. Large Lattices

Including mean-field calculations allows for studying the caloric response for larger lattice sizes and analyzing the convergence of results. Fig. 10(a) presents the spin caloric response as a function of temperature for  $Q = 4$ , and in Fig.(b) for the case of  $Q = 8$  both for lattice sizes of  $3 \times 3$ ,  $8 \times 8$ ,  $16 \times 16$  and  $32 \times 32$  with an initial field of  $B = 0.05$  and a final field of  $B = 1$ . As discussed, the  $Q = 4$  case only presents one transition of type FP to PP, and we therefore see only a peak in the entropy difference, while  $Q = 8$  presents two phase transitions where we see that  $-\Delta S$  is larger when we go from BKT to PP over that from FP to BKT. From both graphs, we notice that there is a convergence of the caloric response already for a  $32 \times 32$  lattice because it presents the same results as a  $16 \times 16$  lattice both for the case of  $Q = 4$  and  $Q = 8$ . It can also be observed by comparing the two graphs that it is still  $Q = 4$  that presents the highest  $-\Delta S/N$  evaluated on the system.

For the completeness of our calculations, we performed a large lattice scan where the thermodynamic properties of the magnetic substance are obtained through the Monte Carlo method and state selection by the Metropolis algorithm, thus obtaining the internal energy and magnetization for fixed external fields. Fixing the external magnetic field of the simulation at 0.05 and 1.00 (in units of J) and calculating the observables with a thermalization of 50000 flips and a set of 100000 iterations for the calculation of thermal averages, the curve of the magnetocaloric effect is obtained for  $L = 16$  and  $L = 32$ . In Fig. 11, we observe the magneto-caloric per spin effect for  $16 \times 16$  and  $32 \times 32$  lattices using mean-field calculations (orange curves) and using the Monte Carlo method (black-grey curves) for the case (a)  $Q = 4$  and (b)  $Q = 8$ . We can observe from there that the Monte Carlo calculation concerning the mean-field calculation coincides with each other in the maximum value of the effect but not in the temperature at which the maximum occurs. It can



(a)

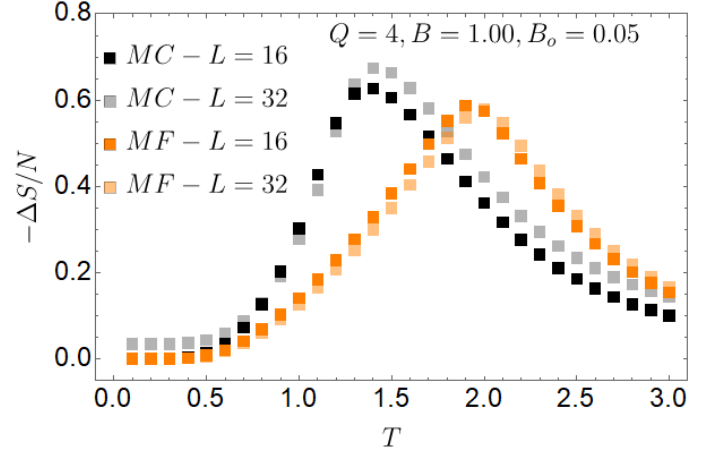


(b)

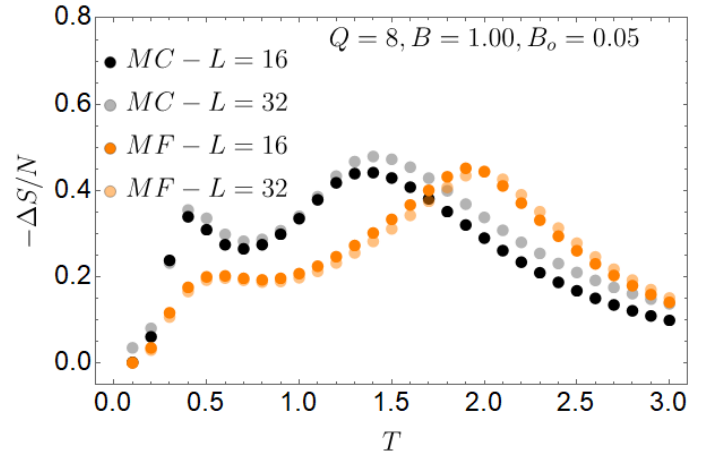
FIG. 10. Mean field calculations for (a)  $Q = 4$  and (b)  $Q = 8$  for  $3 \times 3$ ,  $8 \times 8$ ,  $16 \times 16$  and  $32 \times 32$  lattice.

also be seen that for the case of the Monte Carlo analysis, the  $16 \times 16$  and  $32 \times 32$  effects still show differences with each other (small), while, as we mentioned earlier in the discussions, the mean-field case already converges for a  $32 \times 32$  lattice. However, it is observed that for Monte Carlo simulations up to the location of the first maximum (or the only one for  $Q < 5$ ) corresponding to an FP to PP transition,  $-\Delta S$  presents almost the same values for  $16 \times 16$  and  $32 \times 32$ . However, there is a small difference between the values obtained for these networks near the single transition for  $Q=4$  and from the second transition for  $Q = 8$ .

Finally, returning to the discussion of the phases and their role in quantifying the effect, Fig. 11(a)-(b) shows that for large networks, the peak of the effect is much closer to the BKT-PP type transition, and this is corroborated by both mean-field and Monte Carlo simulations. However, we must reiterate that the opposite occurs in small lattices, where exact calculations have been performed since we observe that the maximum  $-\Delta S$  is close



(a)



(b)

FIG. 11. Magneto-caloric per spin effect for  $16 \times 16$  and  $32 \times 32$  lattices using mean-field calculations (orange curves) and using the Monte Carlo method (black-grey curves) for the case (a)  $Q = 4$  and (b)  $Q = 8$ .

to the FP-BKT type transitions.

## VII. CONCLUSIONS

In this work, we have studied the magneto-caloric effect for a spin system with  $Q$  orientations known as the  $Q$ -clock model. We reviewed the thermodynamic quantities describing the model and calculated for  $Q$  pairs between 2 and 8 using three methods: exact, mean-field, and Monte Carlo simulations. For small lattices ( $3 \times 3$ ) by exact calculations, we have found that there is a region of field where the effects of  $Q = 6$  and  $Q = 8$  are higher than those presented for the cases of  $Q = 4$  and  $Q = 2$ , and then in higher regimes of the external field, they are ordered in descending form as  $-\Delta S_{max}^{Q=4} > -\Delta S_{max}^{Q=6} > -\Delta S_{max}^{Q=8} > -\Delta S_{max}^{Q=2}$ . Forcing the mean-field approximation to explore these lattice

sizes, we note that mean-field allows us to quantify the maximum (in intensity) fairly close to the exact calculation; however, for reasons of applying it to small lattices, it fails considerably in the temperature location where it occurs.

Related to the magnetic phases involved in maximizing the caloric phenomenon, we can report that for small lattices for  $Q \geq 5$ , the FP-BKT transition plays a fundamental role. This changes abruptly when we explore large lattices, where Monte Carlo simulations are employed, which indicate that the transition where the effect is maximized is closer to a BKT-PP type. In addition, there are two considerable effects for large-size lattices: First, there is a convergence of results, evidenced by Monte Carlo and mean-field simulations for lattices

as large as  $32 \times 32$  in the results, and the superior effect always occurs for  $Q = 4$ .

## VIII. ACKNOWLEDGMENTS

M. A., F. J. P., E. V., and P.V acknowledge the financial support of CEDENNA (Chile) under contract ANID AFB220001 and Fondecyt (Chile) under contract 1230055. F. J. P. and P.V. acknowledge support from ANID Fondecyt grant under contract 1240582. F.J.P. acknowledges financial support from “Millennium Nucleus in NanoBioPhysics” project NNBP NNCN2021 .021 and UTFSM DGIIE.

- 
- [1] M. S. Reis and N. Ma, Caloric effects of quantum materials: An outlook, *Physics Open* **4**, 100028 (2020).
- [2] N. R. Ram, M. Prakash, U. Naresh, N. S. Kumar, T. S. Sarmash, T. Subbarao, R. J. Kumar, G. R. Kumar, and K. C. B. Naidu, Review on magnetocaloric effect and materials, *Journal of Superconductivity and Novel Magnetism* **31**, 1971 (2018).
- [3] L. Cirillo, A. Greco, and C. Masselli, Cooling through barocaloric effect: A review of the state of the art up to 2022, *Thermal Science and Engineering Progress* **33**, 101380 (2022).
- [4] B. Li, Y. Kawakita, S. Ohira-Kawamura, T. Sugahara, H. Wang, J. Wang, Y. Chen, S. I. Kawaguchi, S. Kawaguchi, K. Ohara, *et al.*, Colossal barocaloric effects in plastic crystals, *Nature* **567**, 506 (2019).
- [5] D. Matsunami, A. Fujita, K. Takenaka, and M. Kano, Giant barocaloric effect enhanced by the frustration of the antiferromagnetic phase in  $\text{mn}_3\text{gan}$ , *Nature materials* **14**, 73 (2015).
- [6] N. Ma and M. S. Reis, Barocaloric effect on graphene, *Scientific reports* **7**, 13257 (2017).
- [7] F. Xiao, M. Jin, J. Liu, and X. Jin, Elastocaloric effect in  $\text{ni}_{50}\text{fe}_{19}\text{ga}_{27}\text{co}_4$  single crystals, *Acta Materialia* **96**, 292 (2015).
- [8] J. Chen, L. Lei, and G. Fang, Elastocaloric cooling of shape memory alloys: A review, *Materials Today Communications* **28**, 102706 (2021).
- [9] D. Cong, W. Xiong, A. Planes, Y. Ren, L. Mañosa, P. Cao, Z. Nie, X. Sun, Z. Yang, X. Hong, *et al.*, Colossal elastocaloric effect in ferroelastic  $\text{ni-mn-ti}$  alloys, *Physical review letters* **122**, 255703 (2019).
- [10] A. Chauhan, S. Patel, and R. Vaish, Elastocaloric effect in ferroelectric ceramics, *Applied Physics Letters* **106** (2015).
- [11] A. Chauhan, S. Patel, R. Vaish, and C. R. Bowen, A review and analysis of the elasto-caloric effect for solid-state refrigeration devices: Challenges and opportunities, *MRS Energy & Sustainability* **2**, E16 (2015).
- [12] A. Mischenko, Q. Zhang, J. Scott, R. Whatmore, and N. Mathur, Giant electrocaloric effect in thin-film  $\text{pbzr}_0.95\text{ti}_0.05\text{o}_3$ , *Science* **311**, 1270 (2006).
- [13] Y. Liu, J. F. Scott, and B. Dkhil, Direct and indirect measurements on electrocaloric effect: Recent developments and perspectives, *Applied Physics Reviews* **3** (2016).
- [14] T. Correia and Q. Zhang, Electrocaloric effect: an introduction, in *Electrocaloric Materials: New Generation of Coolers* (Springer, 2013) pp. 1–15.
- [15] Y. Jia and Y. Sungtaek Ju, A solid-state refrigerator based on the electrocaloric effect, *Applied Physics Letters* **100** (2012).
- [16] A. M. Tishin and Y. I. Spichkin, *The magnetocaloric effect and its applications* (CRC Press, 2016).
- [17] N. De Oliveira and P. J. von RANKE, Theoretical aspects of the magnetocaloric effect, *Physics Reports* **489**, 89 (2010).
- [18] V. K. Pecharsky and K. A. Gschneidner Jr, Magnetocaloric effect and magnetic refrigeration, *Journal of magnetism and magnetic materials* **200**, 44 (1999).
- [19] V. Franco, J. Blázquez, J. Ipus, J. Law, L. Moreno-Ramírez, and A. Conde, Magnetocaloric effect: From materials research to refrigeration devices, *Progress in Materials Science* **93**, 112 (2018).
- [20] M. S. Reis, Magnetocaloric and barocaloric effects of metal complexes for solid state cooling: Review, trends and perspectives, *Coordination Chemistry Reviews* **417**, 213357 (2020).
- [21] M. Reis, Oscillating magnetocaloric effect on graphenes, *Applied Physics Letters* **101** (2012).
- [22] M. S. Reis, Oscillating magnetocaloric effect, *Applied Physics Letters* **99** (2011).
- [23] M. Reis, Diamagnetic magnetocaloric effect due to a transversal oscillating magnetic field, *Physics Letters A* **378**, 1903 (2014).
- [24] P. Martínez-Rojas, M. E. Benavides-Vergara, F. J. Peña, and P. Vargas, Caloric effect due to the aharonov-bohm flux in an antidot, *Nanomaterials* **13**, 2714 (2023).
- [25] O. A. Negrete, F. J. Peña, and P. Vargas, Magnetocaloric effect in an antidot: the effect of the aharonov-bohm flux and antidot radius, *Entropy* **20**, 888 (2018).
- [26] O. A. Negrete, F. J. Peña, J. M. Florez, and P. Vargas, Magnetocaloric effect in non-interactive electron systems: “the landau problem” and its extension to quantum dots, *Entropy* **20**, 557 (2018).
- [27] O. Tegus, E. Brück, L. Zhang, K. Buschow, F. De Boer, *et al.*, Magnetic-phase transitions and magnetocaloric effects, *Physica B: Condensed Matter* **319**, 174 (2002).

- [28] A. Tishin, K. Gschneidner Jr, and V. Pecharsky, Magnetocaloric effect and heat capacity in the phase-transition region, *Physical Review B* **59**, 503 (1999).
- [29] N. De Oliveira and P. Von Ranke, Magnetocaloric effect around a magnetic phase transition, *Physical Review B* **77**, 214439 (2008).
- [30] V. Franco, A. Conde, M. Kuz'Min, and J. Romero-Enrique, The magnetocaloric effect in materials with a second order phase transition: Are  $t_c$  and  $t_{peak}$  necessarily coincident?, *Journal of Applied Physics* **105** (2009).
- [31] M. Halder, S. Yusuf, M. Mukadam, and K. Shashikala, Magnetocaloric effect and critical behavior near the paramagnetic to ferrimagnetic phase transition temperature in  $TbCo_{2-x}Fe_x$ , *Physical Review B* **81**, 174402 (2010).
- [32] P. J. Shamberger and F. Ohuchi, Hysteresis of the martensitic phase transition in magnetocaloric-effect  $NiMnSn$  alloys, *Physical Review B* **79**, 144407 (2009).
- [33] C. Zhang, D. Wang, Q. Cao, Z. Han, H. Xuan, and Y. Du, Magnetostructural phase transition and magnetocaloric effect in off-stoichiometric  $Mn_{1-x}Ni_xGe$  alloys, *Applied Physics Letters* **93** (2008).
- [34] J. Tobochnik, Properties of the q-state clock model for  $q=4, 5$ , and  $6$ , *Physical Review B* **26**, 6201 (1982).
- [35] Z.-Q. Li, L.-P. Yang, Z. Xie, H.-H. Tu, H.-J. Liao, and T. Xiang, Critical properties of the two-dimensional q-state clock model, *Physical Review E* **101**, 060105 (2020).
- [36] Y. Miyajima, Y. Murata, Y. Tanaka, and M. Mochizuki, Machine learning detection of berezinskii-kosterlitz-thouless transitions in q-state clock models, *Physical Review B* **104**, 075114 (2021).
- [37] C. Lupo and F. Ricci-Tersenghi, Approximating the xy model on a random graph with a q-state clock model, *Physical Review B* **95**, 054433 (2017).
- [38] E. Ilker and A. N. Berker, Odd q-state clock spin-glass models in three dimensions, asymmetric phase diagrams, and multiple algebraically ordered phases, *Physical Review E* **90**, 062112 (2014).
- [39] S. Chatterjee, S. Sutrathar, S. Puri, and R. Paul, Ordering kinetics in a q-state random-bond clock model: Role of vortices and interfaces, *Physical Review E* **101**, 032128 (2020).
- [40] A. Ali, H. Xu, W. Bernoudy, A. Nocera, A. D. King, and A. Banerjee, Quantum quench dynamics of geometrically frustrated ising models, arXiv preprint arXiv:2403.00091 (2024).
- [41] O. A. Negrete, P. Vargas, F. J. Peña, G. Saravia, and E. E. Vogel, Short-range berezinskii-kosterlitz-thouless phase characterization for the q-state clock model, *Entropy* **23**, 1019 (2021).
- [42] O. A. Negrete, P. Vargas, F. J. Peña, G. Saravia, and E. E. Vogel, Entropy and mutability for the q-state clock model in small systems, *Entropy* **20**, 933 (2018).
- [43] M. A. Aguilera, F. J. Peña, O. A. Negrete, and P. Vargas, Otto engine for the q-state clock model, *Entropy* **24**, 268 (2022).
- [44] S. Elitzur, R. Pearson, and J. Shigemitsu, Phase structure of discrete abelian spin and gauge systems, *Physical Review D* **19**, 3698 (1979).
- [45] J. Cardy, General discrete planar models in two dimensions: Duality properties and phase diagrams, *Journal of Physics A: Mathematical and General* **13**, 1507 (1980).
- [46] J. Fröhlich and T. Spencer, The kosterlitz-thouless transition in two-dimensional abelian spin systems and the coulomb gas, *Communications in Mathematical Physics* **81**, 527 (1981).
- [47] G. Ortiz, E. Cobanera, and Z. Nussinov, Dualities and the phase diagram of the p-clock model, *Nuclear Physics B* **854**, 780 (2012).
- [48] Y. Kumano, K. Hukushima, Y. Tomita, and M. Oshikawa, Response to a twist in systems with  $z$  p symmetry: The two-dimensional p-state clock model, *Physical Review B* **88**, 104427 (2013).
- [49] D.-H. Kim, Partition function zeros of the p-state clock model in the complex temperature plane, *Physical Review E* **96**, 052130 (2017).